Received: 11 December 2018 | Revised: 6 August 2019 | Accepted: 21 August 2019

DOI: 10.1002/ldr.3434

WILEY

RESEARCH ARTICLE

Spatiotemporal changes of permafrost in the Headwater Area of the Yellow River under a changing climate

Yu Sheng[1] | Shuai Ma[1,2] | Wei Cao[1] | Jichun Wu[1]

[1] State Key Laboratory of Frozen Soil Engineering, Northwest Institute of Eco-Environment and Resources, Chinese Academy of Sciences, Lanzhou 730000, PR China

[2] College of Resources and Environment, University of Chinese Academy of Sciences, Beijing 100049, China

Correspondence
W. Cao, State Key Laboratory of Frozen Soil Engineering, Northwest Institute of Eco-Environment and Resources, Chinese Academy of Sciences, Lanzhou 730000, PR China.
Email: caowei@lzb.ac.cn

Funding information
National Natural Science Foundation of China, Grant/Award Numbers: 91647103 and 41971093; Subproject of the Strategic Priority Research Program of Chinese Academy of Sciences (CAS), Grant/Award Number: XDA20100103; Self-determined Project Funded by State Key Laboratory of Frozen Soil Engineering, Grant/Award Number: SKLFSE-ZQ-43

Abstract

This article attempts to predict the spatiotemporal changes of permafrost in the Headwater Area of the Yellow River (HAYR) on the northeastern Qinghai-Tibet Plateau, Southwest China by using field monitoring and numerical models. Permafrost in the HAYR is categorized into four types: low- and high-ice-content high-plain permafrost and low- and high-ice-content alpine permafrost. According to these permafrost types, changes in permafrost temperature were calculated by coupling a geometric model with the soil thermal conduction model. Based on the calculation results, this paper evaluates the changes of permafrost in the HAYR over the past 50 years and predicts the change trends of permafrost in the HAYR under the scenarios of RCP2.6, RCP6.0, and RCP8.5 for possible climate change in 2050 and 2010 from the Intergovernmental Panel on Climate Change Fifth Assessment Report. The results show that (a) in the process of permafrost degradation, the same permafrost type at different degradation stages results in different modes and rates of increasing temperature. The response of permafrost to climate change differs in various degradation stages of permafrost; (b) from 1972 to 2012, the areal extent of permafrost degradation was 1,056 km^2, resulting from a sharp air temperature increase after the 1980s. By 2050, the areal extent of permafrost degradation into seasonal frost is similar under the three scenarios of climate change. The areal extent of permafrost degradation is 2,224, 2,347, and 2,559 km^2 or 7.5%, 7.9%, and 8.6% of the total area in the HAYR, respectively. In RCP2.6, the areal extent of permafrost degradation into seasonal frost by 2100 would be approximately 3,500 km^2 greater than that by 2050. In RCP6.0, the areal extent of permafrost degradation by 2100 would be 10,000 km^2 or 32.9% of the total area in the HAYR. In RCP8.5, the area of permafrost degradation by 2100 would be 18,492 km^2 or 62.2% of the total area in the HAYR; (c) the active layer thickness (ALT) in the HAYR would increase significantly. The average of the ALT was 1.51 m by 1972 and 2.01 m by 2012, respectively. Under the RCP2.6, RCP6.0, and RCP8.5 scenarios, the basin-wide average of ALT would be 2.21, 2.40, and 3.08 m by 2050 and 2.78, 4.07, and 4.39 m by 2100, respectively.

KEYWORDS

changing climate, Headwater Area of the Yellow River (HAYR), permafrost, spatiotemporal change

Yu Sheng, Shuai Ma and Wei Cao contributed to the work equally and should be regarded as co-first authors.

1 | INTRODUCTION

Permafrost is defined as ground, including rocks and soil, which contains ice that has been frozen with a temperature at or below 0°C for a period of least two consecutive years. Permafrost is an important component of the cryosphere. It is a type of soil that is sensitive to temperature due to the abundance of underground ice. Permafrost is a special geological body, the evolution of which is unique due to the combined influences of regional landforms, geological structure, lithology, hydrology, and vegetation (Shur & Jorgenson, 2010). It is very sensitive to climatic change and human activity, which may result in the degradation and disappearance of permafrost (e.g., Jorgenson, Shur, & Pullman, 2006; Wu, Zhang, & Liu, 2010; Osterkamp & Romanovsky, 2015). Changes in permafrost affect the climate system by altering water and heat exchanges between the ground and atmosphere and by altering the permafrost carbon stock and subsequently the global carbon cycle (Koven et al., 2011; Schuur et al., 2015; Zimov, Schuur, & Chapin, 2006). In the context of global climate change, the degradation of permafrost and its environmental impacts have thus drawn much attention (Wang, Jin, Li, & Zhao, 2000; Jorgenson, Racine, Walters, & Osterkamp, 2001; Jin, Zhao, Wang, & Jin, 2006; Frey & Mcclelland, 2010; Wu, Sheng, Wu, & Wen, 2010; Yang, Nelson, Shiklomanov, Guo, & Wan, 2010).

Many studies have been conducted on the response of permafrost to climate change. In particular, significant progress has been made in modeling the relationship between permafrost and climate. Many models have been used in predicting spatial changes in permafrost at various scales under different scenarios of climate change (e.g., Azócar, Brenning, & Bodin, 2017; Lu, Zhao, & Wu, 2017; Niu, Yin, Luo, Lin, & Lin, 2018; Wu, Nan, Zhao, & Cheng, 2018; Zhao, Nan, Huang, & Zhao, 2017; Zou et al., 2017). Models for simulating and predicting the spatiotemporal evolution of permafrost can generally be divided into three types: empirical-, empirical-statistical-, and processed-based physical models. Empirical models directly estimate the distribution of permafrost based on historical records (Nelson, 1986, 1987). Empirical-statistical models account factors that influence the distribution of permafrost, such as slope orientation and angle, elevation, air temperature, vegetation, and lithology (Nguyen, Burn, King, & Smith, 2009; Tanarro et al., 2001). Process models use mathematical physics methods and heat transfer principles to simulate the response of permafrost distribution to climate change using data on temperature, soil texture, and soil thermophysical properties (Catherine, Hoelzle, & Haeberli, 2002; Lawrence & Slater, 2005). Empirical and empirical-statistical models only define the presence or absence of permafrost by using topoclimatic and topographic factors, such as the southern boundary of permafrost or the 0°C—isotherm of mean annual air temperature. It is thus difficult or impossible to simulate the change of permafrost at depths. On the other hand, the land-surface process model can only predict the behavior of very shallow depths, ice-water phase change, and simple soil textures. Thus, its capability for simulating and predicting spatiotemporal changes in deep permafrost is greatly limited due to the lack of long-sequence, high-accuracy forcing data (Wang et al., 2016). An alternative to empirical or process-driven models is numerical models, such as those based on finite-element or finite-difference methods. Numerical models can describe heat transfer in the permafrost strata and can help explain the delayed response of permafrost to climate change. They have significant advantages in calculating changes in permafrost temperature governed by thermal conduction, particularly in describing how temperatures change with depth (Riseborough, Shiklomanov, EtzelmÜLler, Gruber, & Marchenko, 2010).

A geographical information system (GIS)-aided elevation model was used to predict future permafrost changes to the Tibetan Plateau. This model was conducted under HadCM2 of general circulation model from the Hadley Centre for Climate Prediction and Research (Li & Cheng, 1999). The results indicate that no more than 19% of permafrost that would disappear over the next 20–50 years. However, this percentage would increase to 58% by 2099. The possible changes of permafrost on the Tibetan Plateau over the next 50 and 100 a have been estimated based on the rising rates of the mean annual air temperature of 0.02 and 0.052°C·yr^{-1} (Nan, Li, & Cheng, 2005). The results suggest that for the two climate warming scenarios, the rates for the reduction of the areal extent of Tibetan permafrost after 50 a would be 8.8% and 13.5%, respectively, and those after 100 a would be 13.4% and 46%, respectively. Some scholars also have estimated permafrost changes on the Tibetan Plateau during the 21st century by using the Community Land Model version 4.0 land-surface model, which predicts a reduction in plateau permafrost extent by approximately 39% by 2050 and 81% by 2100 (Guo, Wang, & Li, 2012). Although some progress has been made in simulating or prediction the distribution of permafrost on the Qinghai-Tibet Plateau, more refined and small-scale models need to be developed for a more accurate assessment of the ecological and hydrological effects caused by climate change (Li et al., 2008; Ran et al., 2012; Ran, Li, & Cheng, 2018).

The Headwater Area of the Yellow River (HAYR) on northeastern the Qinghai-Tibet Plateau, Southwest China, is in a transition zone from discontinuous permafrost to seasonal frost. Under the influence of a warming climate, permafrost in the HAYR has shown regional degradation trend, resulting in a series of ecological and environmental problems (Jin et al., 2009). However, the extent of permafrost degradation and its changing trends remain unknown. Therefore, permafrost in the HAYR is categorized into different types according to its geomorphic units and stratum features. The change processes of permafrost temperature were calculated by coupling a geometric model with the soil thermal conduction model for different types of permafrost. Based on the resulting model, we studied the change process of permafrost in the HAYR over the past 50 years. Additionally, the development trends of permafrost are also predicted under the climate change scenarios of RCP2.6, RCP6.0, and RCP8.5 in 2050 and 2010. The past and future spatiotemporal changes and trends in the HAYR derived from this model can provide a baseline for hydrological and ecological studies and management in a sustainable manner.

2 | MATERIALS AND METHODS

2.1 | Study area

The HAYR (95°55′–98°41′E, 33°56′–35°31′N; 4,193–5,238 m a.s.l.) refers to the catchment area above the Duoshixia Gorge (98°20′ 59.03′E, 34°46′25.15′N; 4,222 m a.s.l.), with an areal extent of 2.97 × 10^4 km^2 (Figure 1). This region has a continental plateau climate. The representative mean annual air temperature was −3.3°C during 1953–2017, as recorded at the Madoi Meteorological Station (98° 18′E, 34°33′N; 4272 m a.s.l.), Qinghai Province, China. Mean annual precipitation and evaporation were 322 and 1,340 mm during 1953–2017, respectively. Numerous meandering rivers, braided streams of the Yellow River, and lakes, such as the Sisters Lakes, Xingxing Hai and Xingxiu Hai lake clusters, are found in the HAYR. The relatively simple vegetation types are dominated by paludal alpine meadows, alpine meadows, steppes, and deserts. The regional topography is characterized by obvious zonal features. Tectonically, the HAYR belongs to the fault basin of the Late Cenozoic in NW–SE directions, which determines the regional topography. The HAYR is surrounded by high mountains at the northern, western, and southern sides. Gentle, lower valleys and lake basins are located in the central region. Quaternary alluvial–proluvial sediments generally cover the basins, intermountain valleys, and the piedmont plain. The sediments are composed of fine- and coarse-grained soils. Additionally, this region is covered by sand, sandy loam, and clay in the upper layer and gravels in the bottom layer (Fang, Zhao, & Sun, 2009). Alpine permafrost is well-developed with a mosaic distribution of zones of seasonal frost and patchy, sporadic, discontinuous, and continuous permafrost on the northeastern Qinghai-Tibet Plateau. The areal extent of permafrost, mainly warm permafrost, is 2.5 × 10^4 km^2, 85.2% of the total area of the HAYR; and that of seasonal frost is 0.3 × 10^4 km^2, 9.8%. The mean annual ground temperature (MAGT) is between −2°C and −0.2°C, and the permafrost thickness may exceed 100 m on mountain tops.

2.2 | Permafrost prediction model

Permafrost changes can be depicted by changes in ground temperature. Thermal conduction is the dominant heat transfer mode in permafrost strata. Surface climate changes drive thermal conduction in the permafrost strata through temperature boundary conditions. For temperature changes in the permafrost strata, a simplified computational model was established under the control of upper and lower thermal boundaries.

2.2.1 | Geometric model

The geomorphological types are complex, and the frozen ground types are diverse in the HAYR. In general, geomorphic units determine the types of stratigraphic sediments and the occurrence and types of ground ice. Therefore, the MAGT, active layer thickness (ALT), and permafrost thickness differ with topographic and geomorphology. Based on the digital geomorphological database of China, on a scale of 1:1,000,000, the landform patterns of the HAYR are classified into 13 categories in the HAYR (Zhou, Cheng, Zhao, Gao, & Nan, 2007). In this study, 13 types of landforms in the HAYR are further merged into two types: high-plain regions and alpine regions. One hundred and one cores of rock were collected by exploration drilling of the permafrost

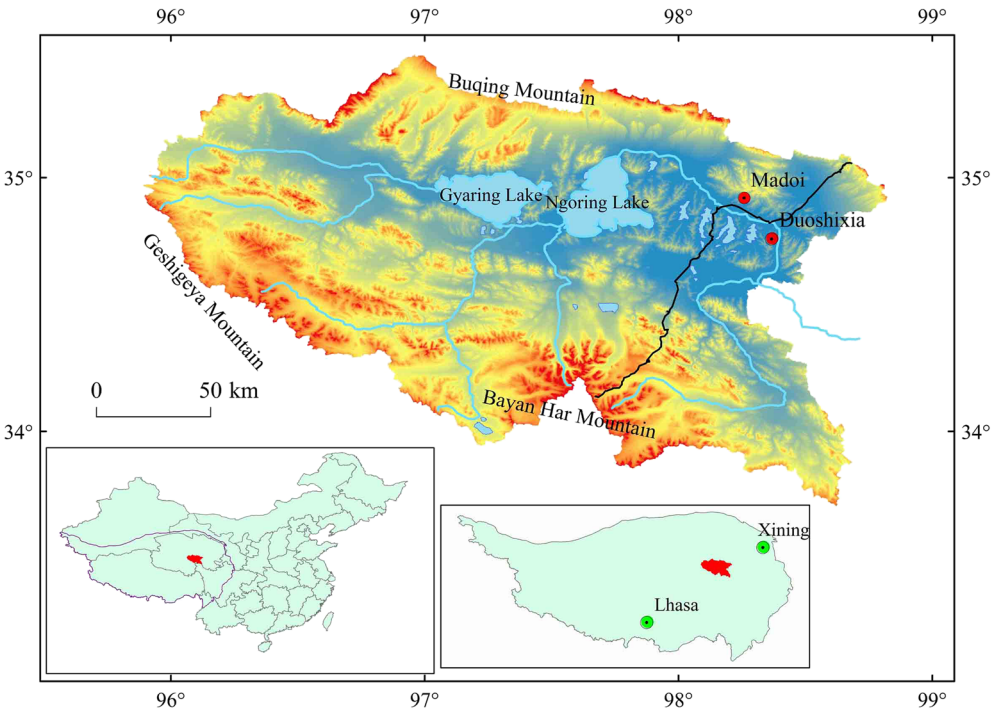

FIGURE 1 Location of the study area [Colour figure can be viewed at wileyonlinelibrary.com]

from 2002 to 2015 in the HAYR. Based on these drilling data, permafrost is classified into five categories in the HAYR according to ice content. These types of permafrost include ice-poor, icy, ice-rich, and ice-saturated permafrost and ice layer with soil inclusions. Usually, ice-rich, ice-saturated permafrost and ice layer with soil inclusions are classified as the high-ice-content permafrost. In this study, the five types of permafrost in the HAYR are further merged into two types: high-ice-content permafrost (HICP) and low-ice-content permafrost (LICP). Drilling data analysis results suggest that the regions of erosional and alluvio-fluvial plains are covered by LICP, whereas the regions of lacustrine-marshland and alluvio-lacustrine plains are covered by HICP. The regions of glacio-periglacial and erosional mountains are covered by LICP, whereas the regions of periglacial mountains and hills are covered by HICP (Wang, Sheng, et al., 2018). Using geomorphic units, stratum features and permafrost characteristics, the permafrost strata in the HAYR are thus categorized into four types: low-ice-content high-plain permafrost (LICHPP), high-ice-content high-plain permafrost (HICHPP), low-ice-content alpine permafrost (LICAP) and high-ice-content alpine permafrost (HICAP). Figure 2 shows the distribution of the four typical permafrost types in the HAYR.

Based on the field investigation of permafrost thickness in the HAYR, a soil depth of 100 m was used for the calculation model. It is hypothesized that variations in ground temperature across the HAYR are constant and thus a one-dimensional model of heat conduction is used for the simulation. According to the analysis and classification of the existing borehole data in the HAYR and the exploratory data along the National Highway 214 from Xi'ning to Yushu, Qinghai Province (Figure 2), the lithology of the four typical permafrost types is shown in Figure 3, which are adopted in the geometric model for simulation, reconstruction, and prediction of permafrost in the HAYR.

2.2.2 | Thermal conduction control equation

Simulation of permafrost changes is performed by a model based on the thermal conduction theory. Permafrost is regarded as a heat conductor in the prediction model. Thus, the simulation only considers the heat conduction of the soil mass and the phase change of ice and water. Heat convection and other effects can be ignored because heat exchange mainly takes place between the soil bodies in a one-dimensional manner. Considering thermal conduction and ice-water phase changes in the soil mass, a physical equation is developed on the basis of energy balance and temperature continuity:

$$C_f\frac{\partial T_1}{\partial t}=\frac{\partial}{\partial x}\left(\lambda_f\frac{\partial T_1}{\partial x}\right),\ C_w\frac{\partial T_2}{\partial t}=\frac{\partial}{\partial x}\left(\lambda_w\frac{\partial T_2}{\partial x}\right), \tag{1}$$

$$T(0,t)=f(t),\ T(x,0)=g(x),\ T_1(x,t)|_{x=\xi}=T_2(x,t)|_{x=\xi}=T_f, \tag{2}$$

$$\lambda_f\frac{\partial T_1}{\partial x}|_{x=\xi}-\lambda_w\frac{\partial T_2}{\partial t}|_{x=\xi}=L\gamma_d(W-W_u)\frac{d\xi}{dt}, \tag{3}$$

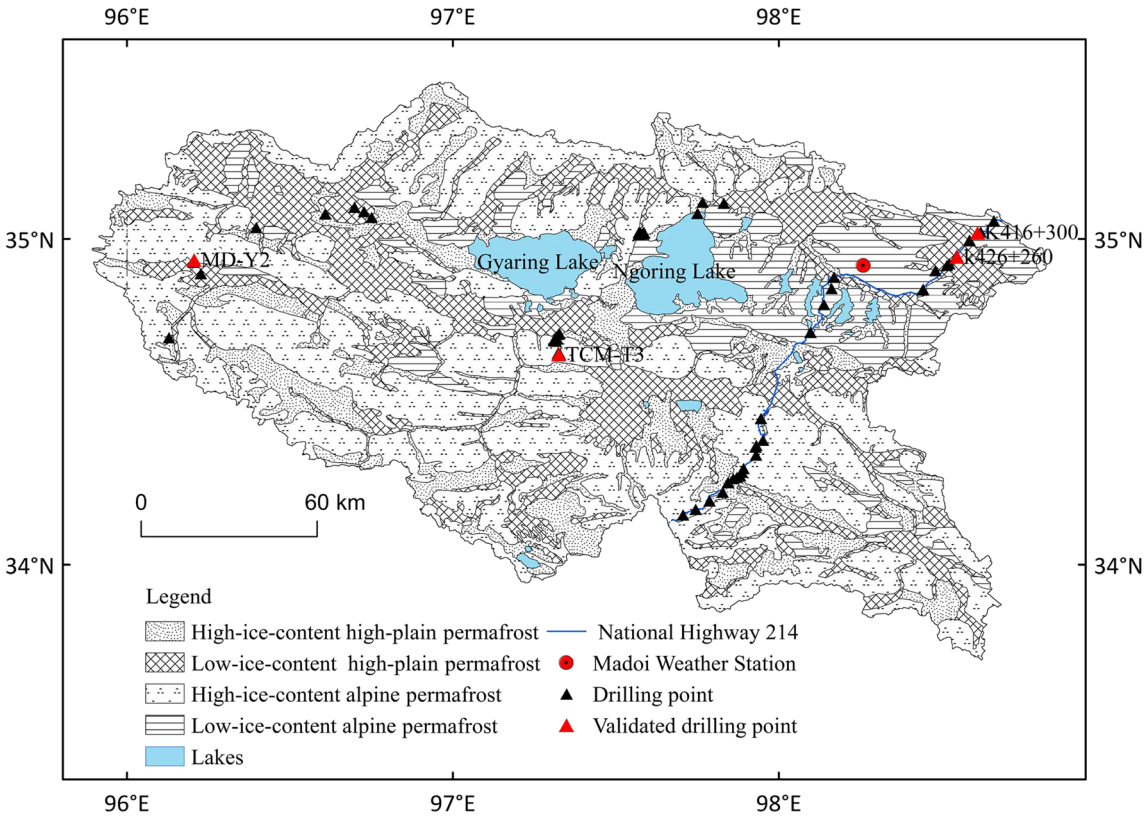

FIGURE 2 Distribution of four typical permafrost [Colour figure can be viewed at wileyonlinelibrary.com]

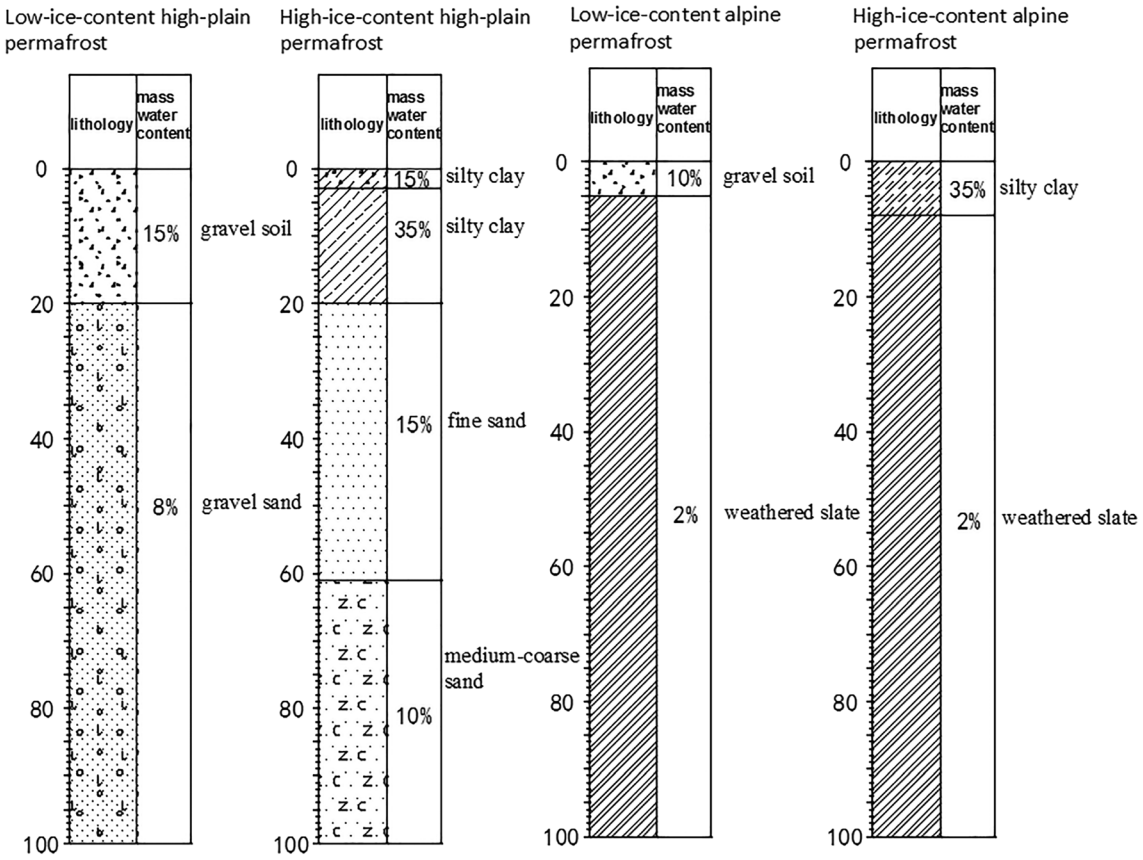

FIGURE 3 Lithology of four representative types in the Headwater Area of the Yellow River

$$T_1(x, t)|_{x=\xi_d} = T_2(x, t)|_{x=\xi_d} = T_f,\ \lambda_w \frac{\partial T_1}{\partial t}|_{x=H} = q, \tag{4}$$

$$\lambda_f \frac{\partial T_1}{\partial x}|_{x=\xi_d} - \lambda_w \frac{\partial T_2}{\partial t}|_{x=\xi_d} = L\gamma_d (W - W_u)\frac{d\xi}{dt}, \tag{5}$$

where λ_f and λ_w are thermal conductivity of permafrost and thawed soil, respectively, (W/(m·°C)); C_f and C_w are thermal capacity of permafrost and thawed soil, respectively, (kJ/(m^3·°C)); and γ_d is dry density of the strata (kg m^{-3}). Additionally, T_1 and T_2 are temperatures of permafrost and thawed zones, respectively, (°C); T_f is the freezing temperature of soil (°C); W and W_u are soil moisture and unfrozen water contents, respectively, (%); and x and t are space and time variables, respectively, (m, s). H is the lower boundary of the computational domain, (m); ξ_d is the lower boundary of permafrost (m), and L is the change in latent heat of water (334.56 kJ/kg). Thermophysical properties of rock and soil (Table 1) in different strata in the model are selected according to the reference of national standard (GB50324-2001, 2014) and laboratory measurement.

TABLE 1 Thermophysical properties of soils and rocks in strata (GB50324-2001, 2014)

Rock stratum	γ_d kg m^{-3}	Mass water content (%)	C_w J/(kg·°C)	C_f J/(kg·°C)	λ_w W/(m·°C)	λ_f W/(m·°C)
Silty clay	1,600	15	1,589	1,276	1.11	1.02
Silty clay	1,400	35	2,300	1,694	1.18	1.93
Weathered slate	2,700	2	750	7,50	2.60	2.60
Gravel sand	1,700	8	1,129	900	1.58	2.06
Gravel soil	1,600	15	1,464	1,129	1.28	1.45
Gravel soil	1,600	10	1,255	1,025	0.89	1.00
Fine sand	1,500	15	1,479	1,099	1.54	2.00
Medium-coarse sand	1,600	10	1,213	941	1.48	1.86

2.2.3 | Phase change analysis

The phase change of ice and water in the permafrost is a nonlinear transient problem that should consider the absorption or release of latent heat. Latent heat is represented by an indicator in the phase-change analysis. The indicator is the enthalpy value with the change of temperature. The change of enthalpy is the integral of the product of density and specific heat to temperature. And the calculation formula is expressed as follows (Cao et al., 2014):

$$\Delta H = \int \rho C(T) \mathrm{d}T = \Delta H_1 + \Delta H_2, \tag{6}$$

$$\Delta H_1 = \rho C(T_2 - T_1), \tag{7}$$

$$\Delta H_2 = L\rho \Delta W_u, \tag{8}$$

where $\Delta H$is the enthalpy value of soil body; ΔH_1 is the heat absorbed due to the temperature rise of soil body; ΔH_2 is the heat absorbed due to the phase transition of ice and water; L is the latent heat of water crystallization or ice-out thaw, and the thermal calculation value is generally 334.56 kJ/kg; ρ represents the dry bulk weight of soil body; $C(T)$ is the heat capacity of soil with the change of temperature T; and W_u is the unfrozen-water content. The latent heat of phase change can be calculated according to the change of unfrozen-water content. The relationship between unfrozen water and temperature is exponential (Xu, Wang, & Zhang, 2001):

$$W_u = a\theta^{-b}, \tag{9}$$

where θ is the absolute value of negative temperature; a and b are constants related to the properties of the soil. Unfrozen-water contents of different types of permafrost can be thus calculated according to the reference value of national standard (GB50324-2001, 2014). The enthalpy values of different types of permafrost can be finally calculated according to the above-mentioned formulas.

2.2.4 | Boundary and initial conditions

The surface energy balance determines the upper heat boundary of the soil layer and surface temperature represents resultant energy balance. In the simulation, surface ground temperature is taken as the upper boundary condition. Surface ground temperature generally changes with seasonal variations of air temperature and can be described as a trigonometric function (Li, Cheng, & Guo, 1996):

$$T = T_0 + c{\cdot}t + A{\cdot}\sin\left(\frac{2\pi}{8760}{\cdot}t + \varphi\right), \tag{10}$$

where T_0 is the initial mean annual ground surface temperature (MAGST, °C); c is the rate of change of surface temperature (°C/hr); A is the annual amplitude of surface temperature that is 12°C (Madoi Meteorological Station, 1953–2012); and φ is the initial phase,which determines the initial time or season in the model. Since the model is calculated from the end of the warm season, then $\varphi = \pi$.

Although ground surface and air temperatures change with similar trends, the relationship between air temperature and the ground temperature of different surfaces varies substantially. The initial MAGST varies across regions with different ground temperatures. Therefore, the initial MAGST differs in computational regions and permafrost types. This study will present the permafrost change in the HAYR over the past 50 years (1953–2012) and in the coming 100 years (2013–2100). The temperature increase from 1953 to 2012 was determined by using the fitting analysis of measured air temperature from the Madoi Meteorological Station in HAYR. Based on Coupled Model Intercomparison Project Phase 5 results in IPCC AR5, the temperature rise trend during 2013 to 2100 was predicted by using a new generation of greenhouse gas emission scenarios, RCP2.6, RCP6.0, and RCP8.5. Because different climate models have different simulation results (Su, Duan, Chen, Hao, & Cuo, 2013; Zhang et al., 2013), we use the average value of temperature rise trend for different climate model simulations under scenarios of RCP2.6 (32 models), RCP6.0 (25 models), and RCP8.5 (39 models; Stocker, Qin, Plattner, et al., 2013). The change trend of surface ground temperature at the upper boundary when T_0 = −0.5°C is thus shown in Figure 4. The change in surface ground temperature in the HAYR can be divided into three stages: (a) 1953–1982, the air temperature declined slowly at a rate of 0.2°C·10 yr^{-1}, (b) 1983–2012, the air temperature increased at a rate of 0.64°C·10 yr^{-1}, and (c) 2013–2100, the air temperature will increase, which varies for different warming scenario models. The mean annual air temperature will increase by 0.57°C by 2040 and then will remain constant under scenarios of RCP2.6. The mean annual air temperature will increase by 1.98°C by 2100 under scenarios of RCP6.0. The mean annual air temperature will increase by 1.19°C by 2045 and then will increase by another 2.62°C by 2100—a total of 3.81°C over 100 a under scenarios of RCP8.5.

In this study, the lower boundary conditions use a constant terrestrial heat flow of 0.0474 J/(m^2·s) (Wang & Li, 1983). The initial temperature is determined by using steady-state processing. In order to stabilize the temperature field, we set the calculation time to 300 years. After the temperature becomes stable, the temperature at the end of 300 a will be assumed to be the same as the temperature at the beginning of 1953. Once the initial temperature at the beginning of 1953 is determined, we will input the temperature change values in upper boundary conditions and the constant value of lower boundary conditions during 1953 to 2100 in the calculation model. For the same scenarios, it is supposed that the surface ground temperature (T) rises at the same rate(c). Seven scenarios using the initial MAGST (T_0) of 0.5°C, 0°C, −0.5°C, −1°C, −2°C, −3°C, and −4°C are thus calculated.

2.2.5 | Calculation results and verification

In order to verify the accuracy of the prediction results, 65 ground temperature measurements were collected by exploration drilling of the permafrost from 2003 to 2015 in the HAYR. The observed values at these boreholes are compared with the simulated results. One representative borehole is chosen in each of the four permafrost types as a clear example to compare the results. Figure 5 shows that the

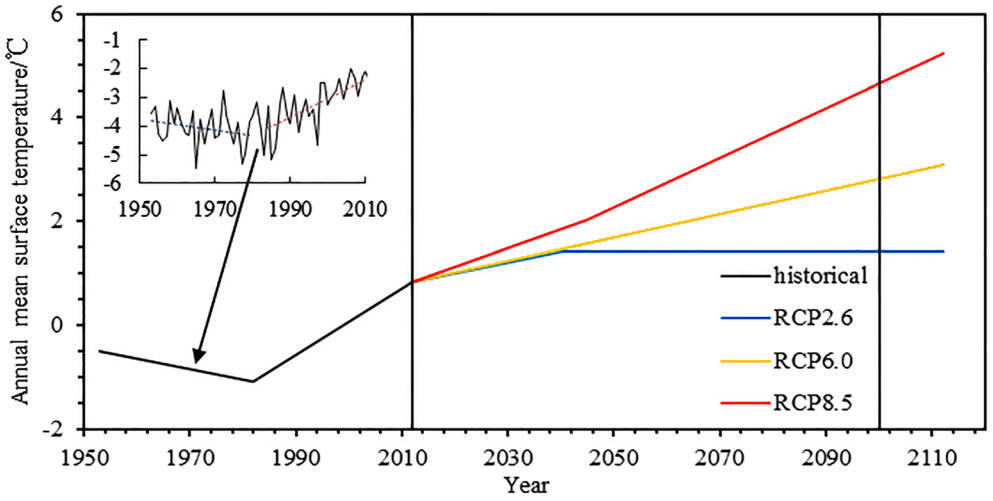

FIGURE 4 Upper boundary temperature rise trend when T_0 = −0.5°C [Colour figure can be viewed at wileyonlinelibrary.com]

change of permafrost temperatures at the boreholes of K426+260 (LICHPP), TCM-T3 (HICHPP), K416 + 300 (LICAP), and MD-Y2 (HICAP). Due to that the time series of the observed ground-temperature data in the HAYR are much shorter, we only collect the monitoring data from permafrost boreholes no more than 10 years. So we compare the observed temperature curve with the simulated temperature curve. The comparison results show that there are differences between the simulated and observed results of ground temperature in the shallow ground. However, the simulated temperature curve of the same permafrost type is in agreement with the observed curve in the deep ground. Especially, the permafrost at the borehole of K416 + 300 is in the zero-gradient stage in the thermal regimes, with a slow temperature rise over the past decade due to phase change (Wu, Zhang, et al., 2010). This means that these calculations of the proposed numerical model are reliable.

2.2.6 | Method of permafrost distribution

Permafrost is a reaction product of heat exchange between the ground surface and the atmosphere. If the heat exchange is constantly in flux between the surface and the atmosphere, the permafrost will constantly change. Ground temperature is an effective index to represent the characteristics of permafrost and therefore is a main indicator of the permafrost zoning. Ground temperatures at the depth of 15–20 m are generally regarded as the MAGT on the Qinghai-Tibet Plateau (Wu, Zhang, et al., 2010). Based on the observed MAGT of permafrost boreholes in 2012, an empirical-statistical MAGT-based model was established by taking account of the latitude, longitude, and elevation as independent variables (Li et al., 2016):

$$GT = 76.59 - 0.20\mathrm{LONG} - 1.16\mathrm{LAT} - 0.0039H \quad R^2 = 0.7659, \quad (11)$$

$$GT_s = GT + 0.3, \quad (12)$$

where GT_s is ground temperature in sunny slope (°C). GT is ground temperature of area expect for a sunny slope (°C); LONG is the longitude (°E); LAT is the latitude (°N), and H is the elevation (m a. s. l.). The sunny slope area is defined as the area with a slope greater than 5°C and a slope direction between 112.5°C and 247.5°C. Based on SRTM DEM data (spatial resolution = 90 m), 0°C is used as the temperature boundary of permafrost and seasonal frost in the HAYR. We can obtain the spatial distribution of permafrost in 2012 (Figure 6) by using the formula (11) and (13). The areal extent of permafrost, mainly warm permafrost, is 2.5 × 10^4 km^2, 85.2% of the total area of the HAYR, and that of seasonal frost is 0.3 × 10^4 km^2, 9.8%.

According to the numerical model simulations, see the previous section, the values of ground temperature at the depths from 0 to 100 m in 1953–2100 can be predicted for the different initial MAGST (T_0). The numerical model was used to calculate the MAGT values with T_0 = 0.5°C, 0°C, −0.5°C, −1°C, −2°C, −3°C, and −4°C. It was found that the value of simulated MAGT (X_{T_0}) in 2012 represents the corresponding grid-zone values of MAGT (X) in the current spatial distribution map of permafrost (Figure 6). The change of the simulated MAGT represents the evolution process of permafrost temperature in these grid zones. Another MAGT values (Y) between the values of simulated MAGT (X_{T_0}) can be linearly interpolated. The calculation formula is given as follows, and the relevant values are calculated.

$$Y = \frac{Y_{-3} - Y_{-4}}{X_{-3} - X_{-4}}(X - X_{-4}) + Y_{-4} \quad X_{-4} \le X < X_{-3}, \quad (13)$$

$$Y = \frac{Y_{0.5} - Y_0}{X_{0.5} - X_0}(X - X_0) + Y_0 \quad X_0 \le X < X_{0.5}. \quad (14)$$

The MAGT values (Y) of permafrost in 1953–2100 in the HAYR can be calculated by the computational formula. The spatial distribution of permafrost in the HAYR can also be presented by overlaying the grid module of ArcGIS. Different MAGT corresponds to different thickness of active layers in the numerical simulation. The ALT can be calculated by using a simple linear relation between the simulated MAGT and ALT. In this study, the calculated ALT represents the average state of the overlying ALT.

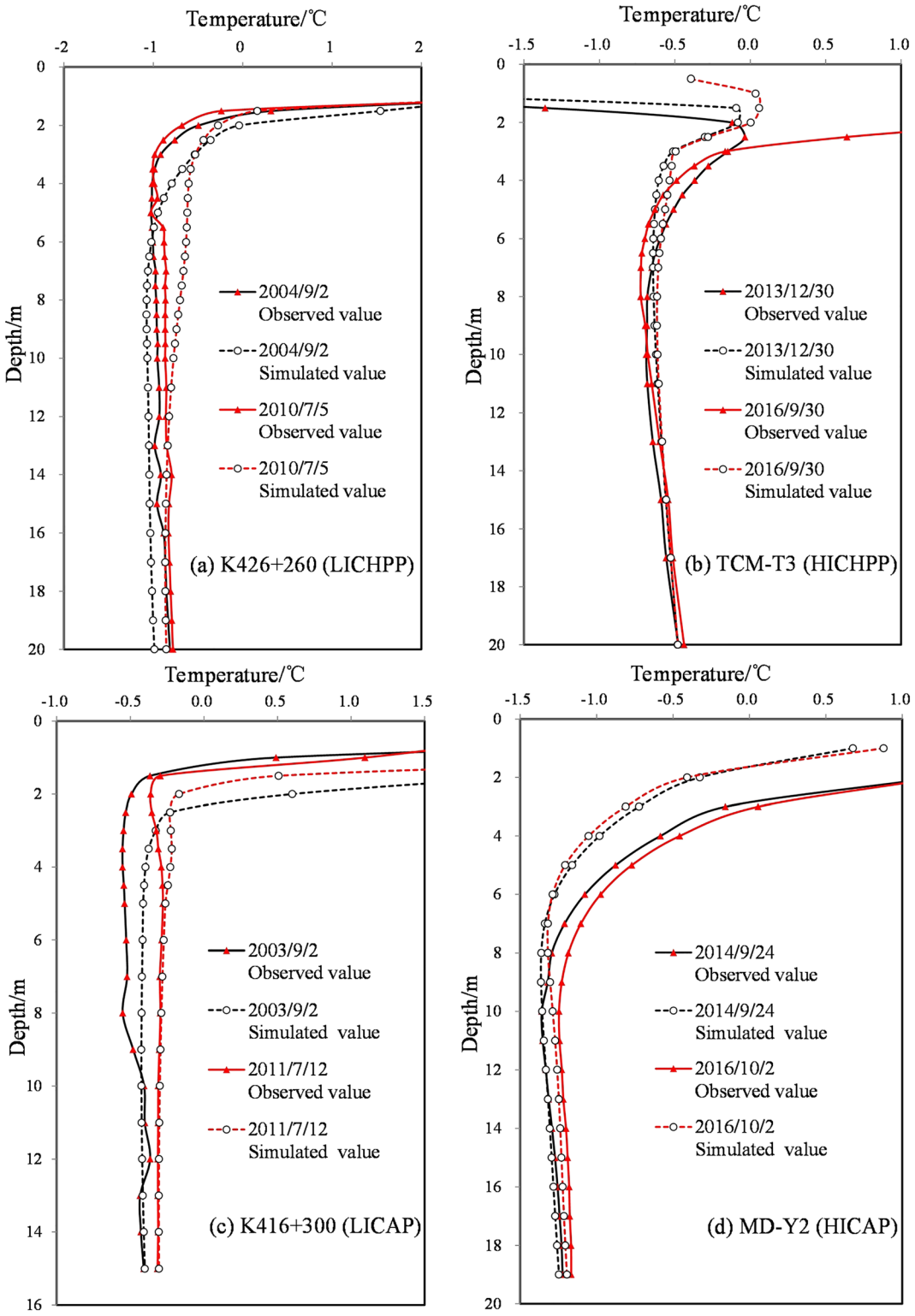

FIGURE 5 Comparison of observed and simulated values of permafrost drilling in the Headwater Area of the Yellow River. HICAP, high-ice-content alpine permafrost; HICHPP, high-ice-content high-plain permafrost; LICAP, low-ice-content alpine permafrost; LICHPP, low-ice-content high-plain permafrost [Colour figure can be viewed at wileyonlinelibrary.com]

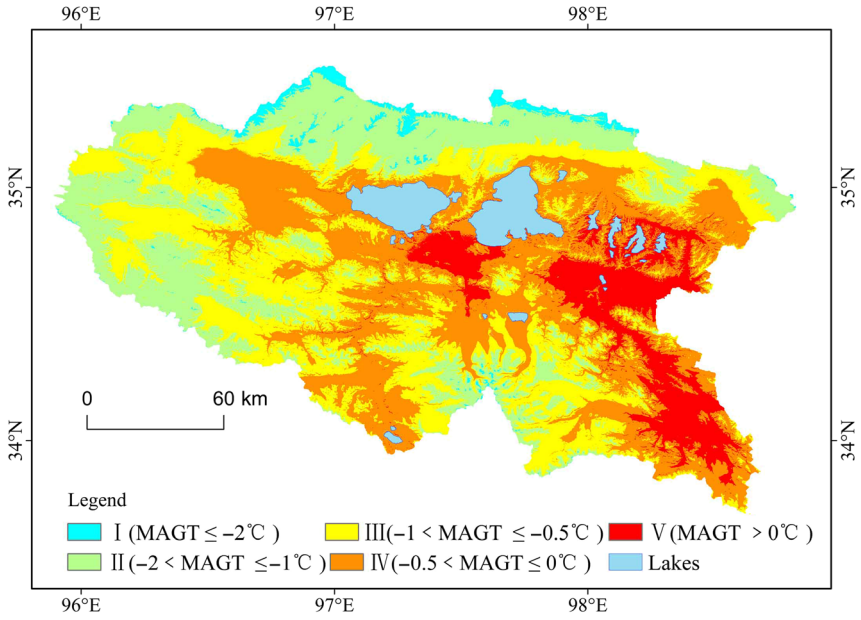

FIGURE 6 Distribution of permafrost in the Headwater Area of the Yellow River of 2012 [Colour figure can be viewed at wileyonlinelibrary.com]

3 | CHANGE PROCESSES OF PERMAFROST UNDER A CHANGING CLIMATE

3.1 | Changes in the temperature of permafrost, table, and base

The degradation stages of the four representative permafrost types in the HAYR can be determined by using the shape of the simulated temperature curves. The changes of ground temperature curves (Figure 7a) and the degradation process (Figure 7b) of the HICAP were plotted under scenario RCP2.6, where the current MAGT is −0.44°C. From 1972 to 2012, the permafrost temperature increased rapidly, accompanied by slight changes in permafrost thickness. From 2013 to 2050, the ground temperature curves were in the zero-geothermal gradient stage. Therefore, the change in ground temperature would be small, and the permafrost thickness would decline quickly from the bottom up. In this stage, the permafrost responds only appreciably to climate warming, because of the dominance of phase change is in thermal regimes. At approximately year 2050, the permafrost would be in the stage of vertical detachment, and a talik would appear, with a downward thawing of permafrost from the lowering permafrost table. After 2085, permafrost would start to disappear. Thawing in all direction would result in the permafrost disappearance.

Moreover, the ground temperature curve also shows the process of permafrost degradation. In the process of permafrost degradation, the same permafrost type, at different degradation stages, results in different modes and rates of temperature increase. The response of permafrost to climate change differs in various degradation stages of permafrost.

Different MAGTs correspond to permafrost thicknesses. Due to differences in MAGTs and permafrost thicknesses, the same type of permafrost can respond to temperature changes at different rates. To determine the influence of MAGT and permafrost thicknesses on the response rates of permafrost to climate changes, three types of permafrost were defined based on the MAGT in 2012: very warm (>−0.5°C), warm (−1 to −0.5°C), and cold (<−1°C) permafrost. As an example of this analysis, the HICAP type of permafrost was used in scenario RCP6. Each of MAGT scenarios is selected from very warm, warm, and cold permafrost for calculations. Changes in the position of the permafrost table and base of the thermal stable types of permafrost are shown in Figure 8. MAGTs of very warm, warm, and cold permafrost were −0.19°C, −0.77°C, and −1.17°C, respectively. The corresponding permafrost thicknesses are 22, 44, and 57 m, respectively. The permafrost table of all three permafrost types experienced a slow and then rapid reduction in permafrost thickness, indicating the detachments of permafrost from seasonal frost (Figure 8). The MAGT increases rapidly once the permafrost layer thaws. Simultaneously, the base of permafrost increases by varying degrees, with the rate of elevation of the permafrost base positively related to the MAGT. Overall, very warm permafrost responds sensitively to climate changes. The thin permafrost would develop a talik layer by 2040; the permafrost table would lower rapidly; and the permafrost would thaw completely by 2060. The warm permafrost would form a talik layer by approximately 2080, and the permafrost would take a long time to thaw. In the cold permafrost, the permafrost table would enter a stage of rapid lowering by approximately 2090, and the permafrost base would rise gradually.

3.2 | Permafrost changes under different conditions

Model calculation results for LICHPP and HICHPP under the scenario RCP2.6 are shown in Figure 9a,b, respectively. For LICHPP permafrost, the ice content is 15% at 0–20 m and 8% at 20–100 m. For HICHPP permafrost, ice content is 15% at 0–3 m, 35% at 3–20 m,

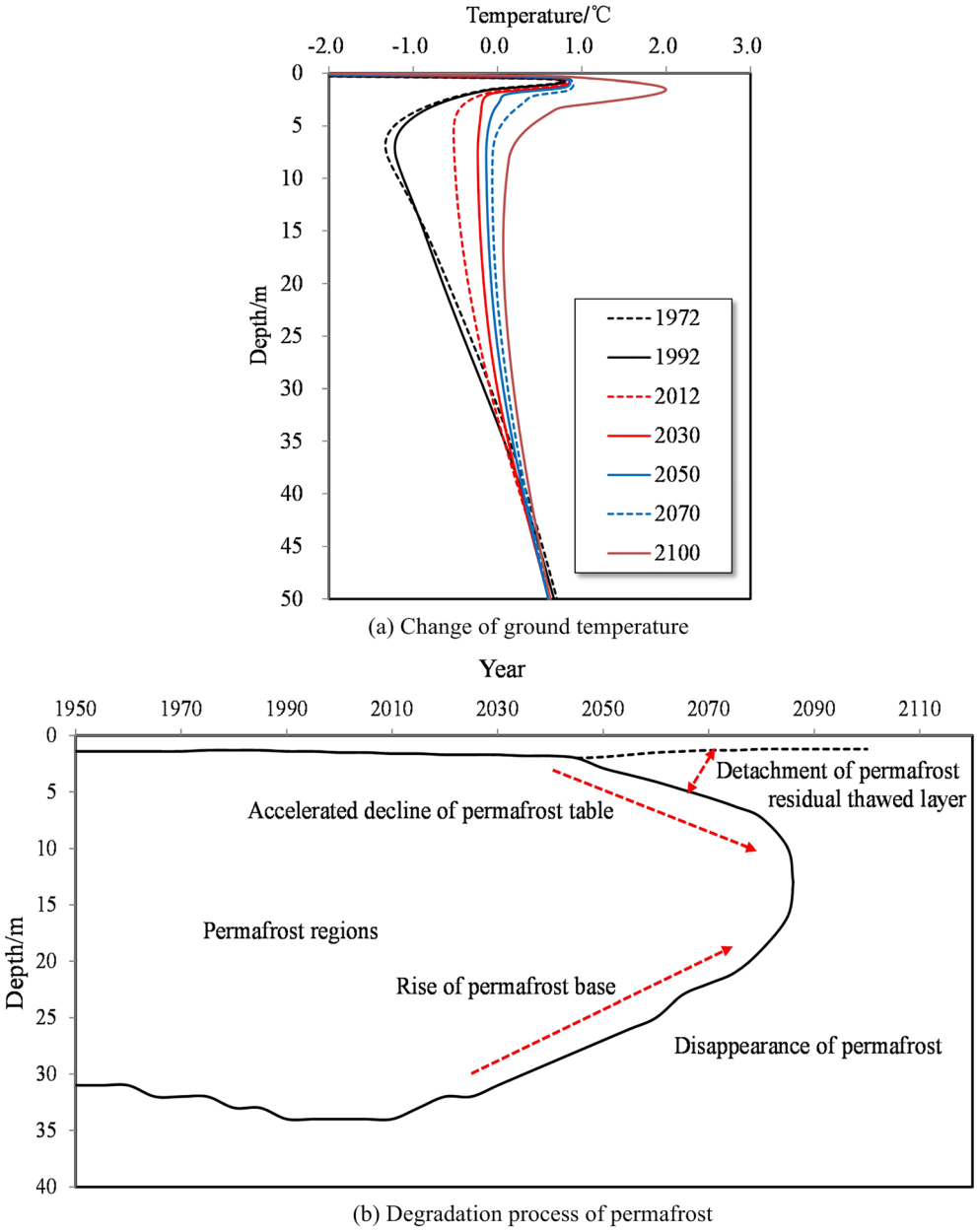

FIGURE 7 Ground temperature curve and degradation process of permafrost [Colour figure can be viewed at wileyonlinelibrary.com]

15% at 20–60 m, and 10% at 60–100 m. The current MAGTs of LICHPP and HICHPP are −0.24°C and −l0.25°C, respectively (Figure 9). Compared with HICP, LICP would have a greater response to climate change and would degrade more easily. The majority of residual permafrost is HICP and pure ice. For example, in Qingshuihe Riverside, the LICP, under similar conditions, would degrade completely. LICP, with the current MAGT of −0.24°C, would thaw completely during the 21st century. Although the ground temperature of HICP at different depths would rise, by a varied extent, the permafrost table and base would change only slightly, and the permafrost table would lower slowly during the late 21st century. Given the same conditions, LICP would degrade more quickly than HICP.

Model results of LICHPP and LICAP under the scenario RCP2.6 are shown in Figure 9c,d, respectively. The current MAGTs of LICHPP and LICAP are −0.24°C and −0.23°C, respectively. There would be a small difference in decay time between these two permafrost types. The degraded alpine permafrost would be thicker. The LICAP has a thin unconsolidated formation, beneath which bedrocks with low ice content are found. Compared with the LICHPP, the ice content of the soil layer is slightly lower in LICAP. The permafrost base depth of the LICHPP would be approximately 24 m, and the permafrost would thaw completely by 2090. The permafrost base depth of the LICAP would be 36 m, and the permafrost will completely thaw by 2070.

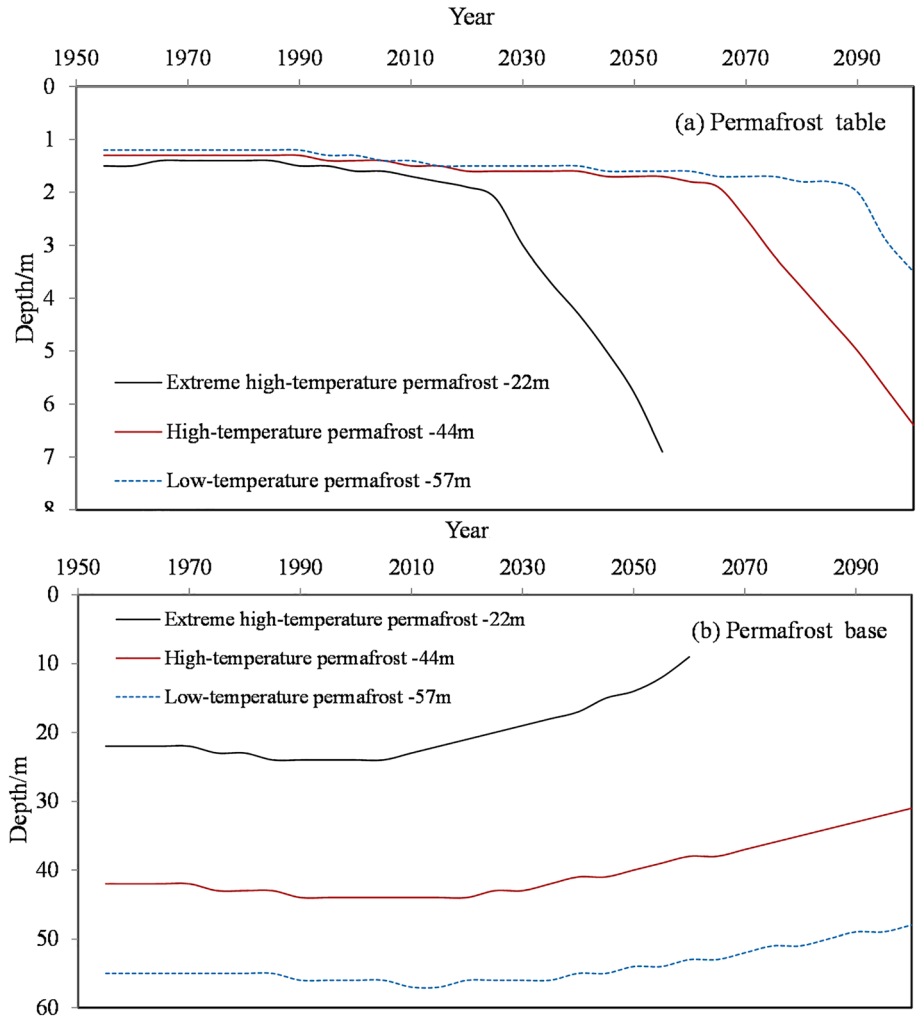

FIGURE 8 Changes of permafrost table and permafrost base with different permafrost thicknesses [Colour figure can be viewed at wileyonlinelibrary.com]

4 | CHANGES IN PERMAFROST DISTRIBUTION

Prior to 1953, an upper boundary condition with constant temperature was used to develop a stable temperature field in the simulation model. However, the changing temperature boundaries were measured at weather stations, and their trends were only incorporated into the model after 1953. Therefore, the simulation results in the few years after 1953 did not reflect the response to previous climate changes and the simulation results deviated from the measured temperature. Therefore, the simulated ground temperature in 1972 was considered closer to the actual temperature, and the decadal changes in permafrost temperatures were compared for years of 1972, 1982, 1992, 2002, and 2012. The simulation was also used to predict the changes in the spatial distribution of permafrost in the HAYR under scenarios RCP2.6, RCP6.0, and RCP8.5 in 2050 and 2100. The distribution of MAGTs is divided for frozen-ground zones at the intervals of 0.5°C and 1.0°C. A total of five ground temperature zones are identified: Zone I (MAGT≤−2.0°C), Zone II (−2.0°C < MAGT ≤ −1.0°C), Zone III (−1.0°C < MAGT ≤ −0.5°C), Zone IV (−0.5°C < MAGT ≤ 0°C), and Zone V (MAGT > 0°C). The change in the spatial distribution of permafrost is computed for the HAYR during different time periods.

4.1 | Changes in the spatial distribution of permafrost in the HAYR over the past 50 years

Based on model reconstruction, the areal extents of permafrost in the HAYR were 2.60×10^4 km^2 in 1972, 2.62×10^4 km^2 in 1982, 2.64×10^4 km^2 in 1992, and 2.62×10^4 km^2 in 2002 (Figure 10). Currently, the areal extent of permafrost in the HAYR is 2.54×10^4 km^2. The results indicate that some seasonal frost was converted into permafrost from 1972 to 1992. The increase in permafrost areal extent during this period was 323 km^2, due to a short cooling period from the 1960s to the 1980s. In contrast, the areal extent of permafrost degradation was 1,056 km^2 from 1992 to 2012, due to sharp warming since the 1980s. The adopted upper boundary temperature began to increase in 1982; however, the permafrost area decreased in 1992, demonstrating the delayed response of permafrost to climate change.

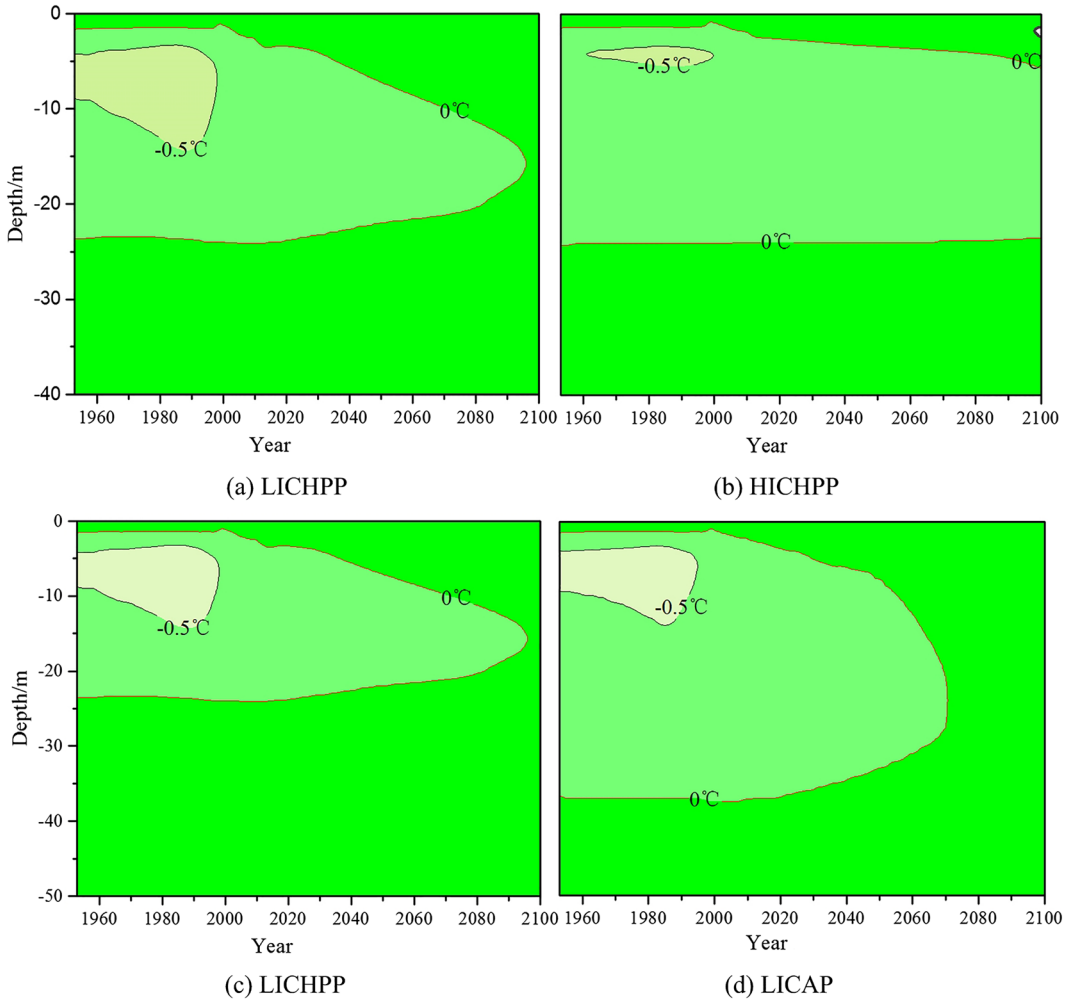

FIGURE 9 Permafrost degradation process with different ice-containing characteristics. HICAP, high-ice-content alpine permafrost; HICHPP, high-ice-content high-plain permafrost; LICAP, low-ice-content alpine permafrost; LICHPP, low-ice-content high-plain permafrost [Colour figure can be viewed at wileyonlinelibrary.com]

Permafrost responses to climate changes can be delayed by more than 10 years or more.

Seasonal frost is mainly found in the Requ Valley in the southeastern HAYR and the Xiaoyemaling and Tangchama piedmont plain in the southern Sisters Lakes Basin. The topography consists primarily of valleys, plains, and flat regions. There are very warm regions of permafrost (Zone IV) at the margins of the seasonal frost. Generally, only small areas of permafrost have been converted into seasonal frost over the past 50 years. During this time MAGTs, of different permafrost types, increased by varying extents. From 1972 to 2012, the areal extent ratio of very warm permafrost (Zone IV) to total permafrost increased from 22.3% to 35.3%. The ratio of warm permafrost (Zone III) increased from 23.4% to 35.3%. The ratio of cold permafrost (Zones I and II) decreased from 54.3% to 29.4%. Although the changes in total permafrost extent are minor, the air temperature increased dramatically in the 1980s, resulting in a significant rise in permafrost temperature. As a result, the cold permafrost was transformed into warm and very warm permafrost.

Changes in the ALT greatly affect ecosystems, ground-atmosphere water balance, and the carbon cycle in permafrost zones. In the HAYR, the average ALT was 1.51 m in 1972, 1.64 m in 1992, and 2.01 m in 2012 (Figure 11). The change ALT was 0.65 cm·yr^{-1} from 1972 to 1992 and 1.85 cm·yr^{-1} from 1992 to 2012. Air temperature increased quickly after 1982, accelerating the increase in ALT in the last 20 years. With an increase in the upper boundary temperature, the ALT increased continuously. From 1972 to 2012, permafrost areas with changes of 0–0.3, 0.3–0.6, 0.6–1, and 1 m in ALT accounted for 47%, 33%, 17%, and 3% of the current permafrost area in the HAYR, respectively. Permafrost types differ in MAGT and surface soil textures and therefore also experience varied changes of the ALT. However, the overall trend, regardless of permafrost type, was a continuous increase.

4.2 | Future spatial distribution changes of permafrost in the HAYR

4.2.1 | Permafrost changes

RCP2.6

In 2050, the permafrost area under scenario RCP2.6 would be 2.32 × 10^4 km^2 (Figure 10e). About 2,224 km^2 of permafrost, 7.5% of the

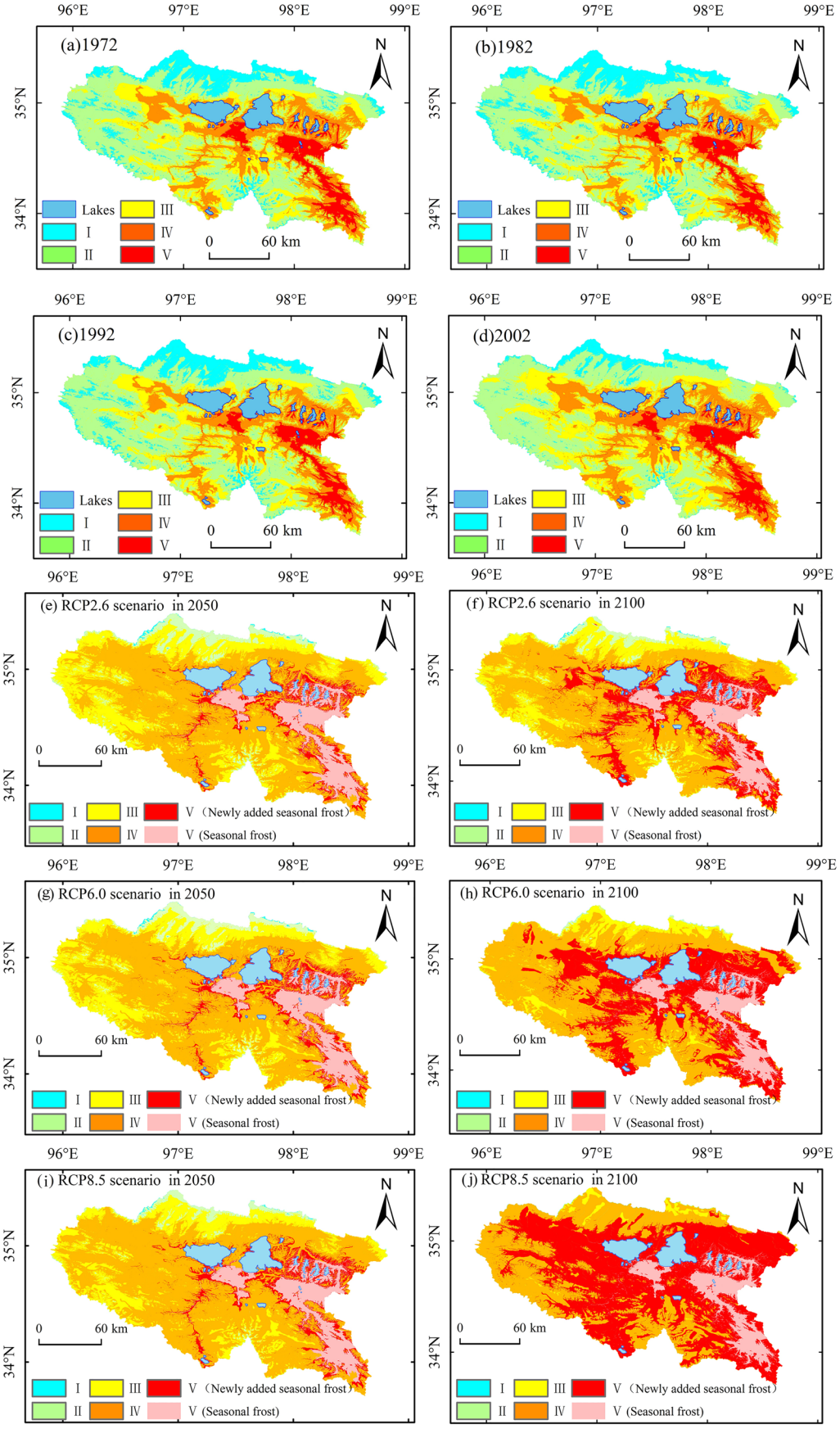

FIGURE 10 Spatial distribution of permafrost in the Headwater Area of the Yellow River under a changing climate [Colour figure can be viewed at wileyonlinelibrary.com]

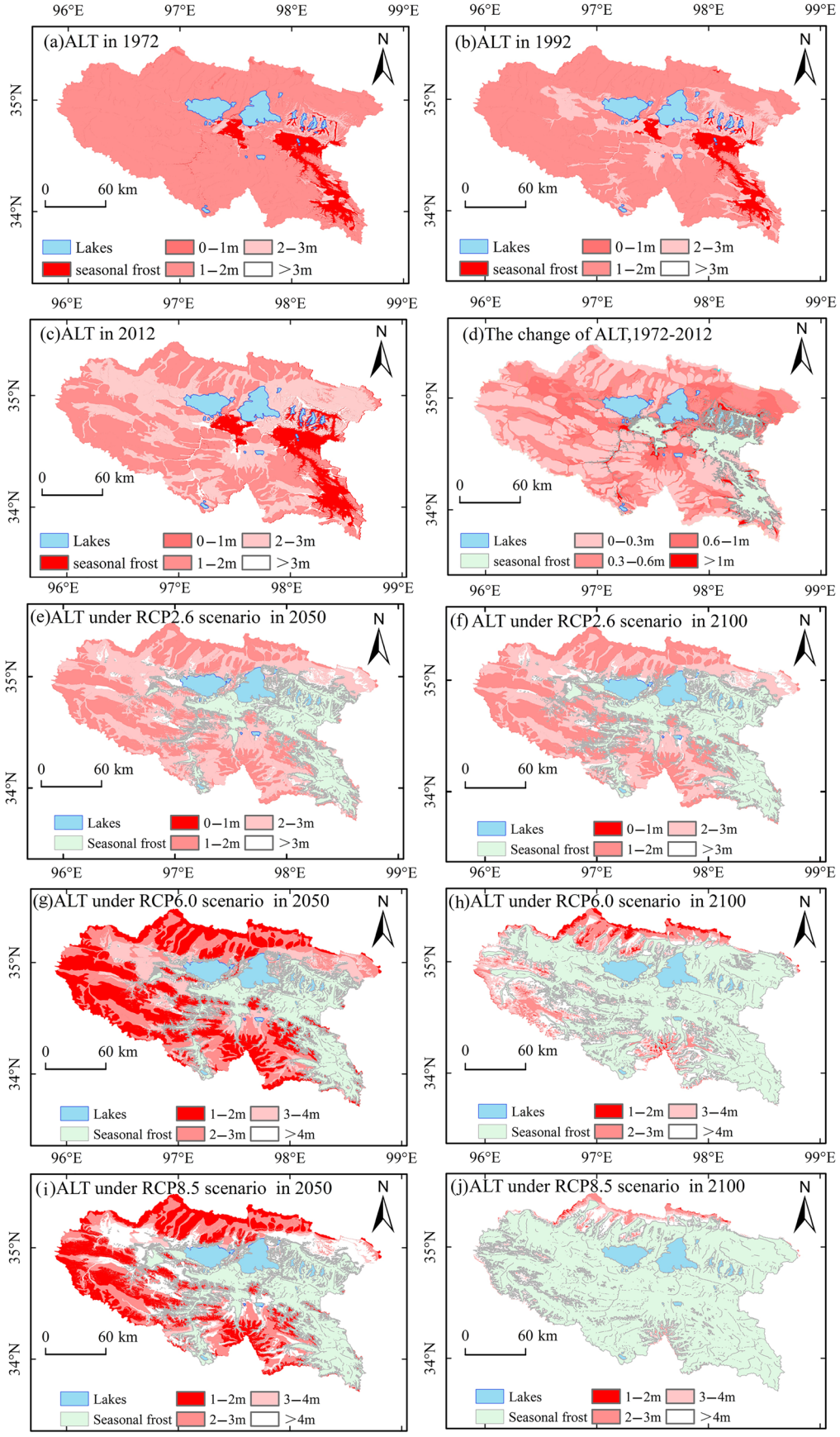

FIGURE 11 Spatial distribution of ALT in the Headwater Area of the Yellow River under a changing climate. ALT, active layer thickness [Colour figure can be viewed at wileyonlinelibrary.com]

total area in the HAYR, would be converted into seasonal frost. There would be very warm permafrost at the edges of both permafrost and seasonal frost. Seasonal frost would be scattered throughout the flat regions, such as Baimaqu, Duoqu, and Maduosihu. The proportion of very warm permafrost to the total permafrost area would increase by 28.5%, whereas those of warm permafrost (Zone III) and cold permafrost (Zones I and II) would decrease by 6.4% and 22.1%, respectively. The very warm permafrost (Zone IV) would then account for 63.8% of total permafrost area in the HAYR.

The air temperature would remain unchanged after 2040; however, permafrost degradation would continue. The permafrost area would shrink to 1.96×10^4 km^2, reflecting the continued but lagged response of the permafrost temperature to previous air temperature rises. The areal extent of permafrost degradation into seasonal frost, from 2050 to 2100, would be approximately 3,500 km^2 (Figure 10f). Specifically, extensive formation of seasonal frost would occur in the Xingxiuhai Wetlands. The Kariqu Basin would change from Zone III into Zone IV. In 2100, very warm permafrost would account for 71.6% of the total permafrost area in the HAYR and warm permafrost for 22.8%. A small areal extent of cold permafrost, only 5.6% of the total permafrost area, would be found in alpine regions (e.g., the Buqing Mountain) in the northern HAYR.

The LICHPP, with the current MAGT greater than −0.10°C, would completely thaw by 2050. Complete thawing of HICHPP, LICAP, and HICAP would occur in zones with current MAGTs higher than −0.02°C, −0.33°C and −0.21°C, respectively. By 2100, compete thawing of LICHPP, HICHPP, LICAP, and HICAP would occur in zones with current MAGTs higher than −0.26°C, −0.15°C, −0.53°C, and −0.44°C, respectively. Therefore, permafrost areas with the MAGT higher than −0.02°C will thaw completely by 2050, and areas with current MAGT higher than −0.15°C will thaw completely by 2100.

RCP6.0

Under scenario RCP6.0, the permafrost area in 2050 would be 2.30×10^4 km^2 (Figure 10g). The area of thawed permafrost would be 2,347 km^2, 7.9% of the total area of the HAYR. Very warm permafrost (Zone IV), warm permafrost (Zone III), and cold permafrost (Zones I and II) would occupy for 66.8%, 26.9%, and 6.3% of the total permafrost area in the HAYR, respectively. The LICHPP permafrost with MAGTs higher than −0.10°C will thaw completely by 2050. The complete thawing of HICHPP, LICAP, and HICAP would occur in zones with current MAGTs greater than −0.02°C, −0.33°C, and −0.21°C, respectively.

The thawed permafrost area in 2100 will be approximately 10,000 km^2, accounting for 32.9% of the total area in the HAYR (Figure 10h). Seasonal frost will be formed extensively in areas such as at Gamale and Duogerong Basins. Moreover, the seasonal frost in the Xingxiuhai Wetlands will expand into the Gyaring Lake Basin. The seasonal frost in the Baimaqu, Lenaqu, and Zhoumaqu Basins will merge. Zone IV permafrost would cover 85.8% of the total permafrost area. Zone III permafrost would cover 13.5% of the total permafrost area, mainly on the higher parts of the Buqing Mountains in the northern HAYR. The proportion of cold (<−1°C) permafrost in the HAYR would be very small, and most permafrost areas would be warmer than −1°C, mainly very warm and warm permafrost. Complete thaw of LICHPP, HICHPP, LICAP, and HICAP would occur in zones with current MAGTs higher than −0.26°C, −0.21°C, −1.05°C, and −0.61°C, respectively. Under the RCP6.0 scenario, in areas with a current MAGT higher than −0.02°C, the permafrost will be thawed completely by 2050, and those warmer than −0.21°C will be thawed completely by 2100.

RCP8.5

Under scenario RCP8.5, the temperature will increase by approximately 4°C. This sharp temperature increase will result in significant permafrost degradation. In 2050, the area of thawed permafrost would cover 2,559 km^2, 8.6% of the total area in the HAYR (Figure 10i). This is similar to the results of the RCP2.6 and RCP6.0 scenarios. In 2050, some permafrost would be in the zero-gradient stage of degradation, and since heat is required for phase change, there would be insignificant changes to the permafrost area. Very warm permafrost (Zone IV), warm permafrost (Zone III), and cold permafrost (Zones I and II) would account for 74.5%, 21.7%, and 3.7% of the total permafrost area in the HAYR, respectively. Although the permafrost area under scenario RCP8.5 is similar to that under the scenario RCP2.6 and RCP6.0, the proportion of very warm permafrost would increase, whereas the proportion of warm permafrost and cold permafrost would decrease. The ground temperature of all permafrost types would continuously increase. Complete thawing of LICHPP, HICHPP, LICAP, and HICAP would occur in zones with MAGTs higher than −0.1°C, −0.08°C, −0.37°C, and −0.21°C, respectively.

A long-term sharp increase in temperature would result in the quick degradation of permafrost in the HAYR. In 2100, the permafrost area under scenario RCP8.5 would be 9,838 km^2, which accounts for approximately 34.7% of the total area in the HAYR (Figure 10j). There would be small areas of permafrost in the north of the Hunan-Hubei Basin and west of the HAYR. The HAYR would primarily contain seasonal frost. Cold permafrost (Zones I and II) would disappear, and more than 90% of the area in the HAYR would be very warm permafrost (Zone IV), with less than 10% containing warm permafrost (Zone III). Complete thaw of LICHPP, HICHPP, LICAP, and HICAP would occur in zones with current MAGTs higher than −0.64°C, −0.38°C, −1.69°C, and −0.96°C, respectively.

4.2.2 | Changes in the ALT

RCP2.6

Under the RCP2.6 scenario, the average ALT in the HAYR would increase to 2.21 m by 2050, 0.2 m greater than in 2012 (Figure 11e). The rate of increase in the ALT would be 0.52 cm·yr^{-1}. In 2100, the average ALT in the HAYR would increase to 2.78 m, 0.77 m greater than in 2012 (Figure 11f). The rate of increase of ALT would be 0.86 cm·yr^{-1} from 2012 to 2100. The ALT in 2050 and 2100 would be 1–3 m. Between 2012 to 2050 and 2012 to 2100, the ALT in the HAYR would have changed by 0–0.6 m. The areal extent of zones with

ALT changes greater than 1 m would expand. From 2012 to 2050, permafrost areas with changes of the ALT greater than 0.6 m would transform into seasonal frost or discontinuous permafrost. Although the upper boundary temperature would remain unchanged after 2040, the active layer would continue to deepen.

RCP6.0

Under scenario RCP6.0, the area of permafrost with an ALT greater 3 m will increase by 2050, mainly in the Xingxiuhai Wetlands to the west of the Gyaring Lake and the western and southern HAYR. The permafrost will thaw completely by 2100. However, in the northern HAYR region, the ALT in most permafrost areas would be smaller than 3 m. The average ALT would be 2.40 m in 2050, 0.38 m greater than that in 2012 (Figure 11g). The rate of increase of ALT was 1 cm·yr^{-1}. The average ALT would be 4.07 m in 2100, 2.06 m greater than that in 2012 (Figure 11h). The change rate would be 2.34 cm·yr^{-1}. The annual rate of change in ALT would increase from 2050 to 2100. The change rate of ALT from 2012 to 2050, under scenario RCP6.0, would be significantly higher than that under scenario RCP2.6. The permafrost zones, with an ALT change greater than 0.6 m, would expand. The change in ALT from 2012 to 2100 would be greater than 0.6 m and permafrost areas, with an ALT increase greater than 1 m, and would occur extensively.

RCP8.5

Changes in ALT would be the greatest under scenario RCP8.5. The average ALT in 2050 would increase to 3.08 m, 1.07 m greater than that in 2012 (Figure 11i). The change rate would be 2.82 cm·yr^{-1} from 2012 to 2050. The average ALT in 2100 would be 4.39 m, 2.38 m greater than that in 2012, a 2.70 cm·yr^{-1} increase from 2050 to 2100 (Figure 11j). In 2100, most areas of the HAYR would be in zones of seasonal frost or discontinuous permafrost, accounting for approximately 90% of the land area in the HAYR. Ecologically and hydrologically, under the scenario RCP8.5, the seasonal frost and deeply buried permafrost would function similarly. The ALT would increase by more than 0.6 m from 2012 to 2050 and by more than 1 m in most permafrost areas from 2012 to 2100.

5 | DISCUSSION

5.1 | Evidence of permafrost degradation

Climate change over the past 60 years has been divided into two stages: (a) a mild cooling from the 1950s to the early 1980s and (b) a marked warming from the early 1980s to the present. The permafrost in the HAYR reacted according to the different trends of climate change, but not significantly. Only 2% of the permafrost area was altered. The area of permafrost in the HAYR has increased since the 1950s, reaching its maximum in the early 1990s, when it then began to decrease.

It is a fact that permafrost in the HAYR is degrading. The meteorological data show that the mean annual air temperature in Madoi County declined slightly from the 1950s to 1980s but has continued to rise since 1980s, at a rate of about 0.08°C·yr^{-1}. During this period, the shallow ground temperature increased from 0.3°C to 0.7°C. The seasonal frozen depth decreased from 3.12 to 2.18 m, a change of nearly 1 m. This indicates a shortening of the frozen period and that permafrost may disappear due to the increase of ground temperature. Moreover, during a field survey in 1991, buried permafrost layers were found to have been exposed in the Xingxinghai lakeshore, the southern beach of Heiheqiao, and the piedmont diluvial fan of Yeniugou. However, none of these areas appeared during in-situ reconnaissance in 1998. It shows that the permafrost layer has degraded.

Moreover, field measurement data shows that there are obvious signs of permafrost degradation in the HAYR. The permafrost table, measured by field drilling, in the alpine or plain areas, has exceeded the maximum frozen depth. This indicates that the permafrost has, in fact, detachment from the frozen ground, which is the most obvious sign of permafrost degradation. The temperature measurements of the boreholes show that the permafrost table is below 5.0 m, which is much larger than the frozen depth of seasonally frozen soil in this area. The altitudes of the boreholes in the region of detached frozen ground are similar to the boreholes in the region of seasonal frozen soil. Moreover, according to the ground temperature curve, the geothermal gradient of most permafrost borehole in the region have approached or reached a zero gradient. The values of ground temperature of some permafrost boreholes have approached 0°C, indicating that the permafrost is on the edge of thawing.

Ground temperature measurement can indicate the permafrost thickness. The results show that the permafrost thickness does not exceed 20 m in low altitude areas, a sign of permafrost degradation. Permafrost degradation is most prominent in several permafrost boreholes in the area of Tangchama (Figure 12).

5.2 | Accuracy of this model forecast result

The fate of the HAYR permafrost is an important scientific issue that is widely debated and remains uncertain. At present, scholars have used various land surface models or numerical simulation methods to predict the future changes of permafrost in the Qinghai-Tibet Plateau under different climate model warming scenarios (Guo et al., 2012; Li et al., 1996; Li & Cheng, 1999; Nan et al., 2005; Wang et al., 2019). The study of Li and Cheng (1999) shows that the permafrost on Qinghai-Tibet Plateau will minimally change in the next 20–50 years. However, it will significantly degrade in 2099, with the proportion of 58.18%. The results of Nan et al. (2005) show that the rate of reduction Tibetan permafrost after 50 a would be 8.8–13.5% and after 100 a would be 13.4–46%. The study of Guo et al. (2012) indicates that a reduction of Qinghai-Tibet plateau permafrost extent by approximately 39% by 2050 and 81% by 2100. The result of Wang et al. (2019) indicates respectively 25.9% and 43.9% of the current permafrost on the Tibetan Plateau will disappear by the 2040s and the 2090s. In this study, the area proportion of permafrost

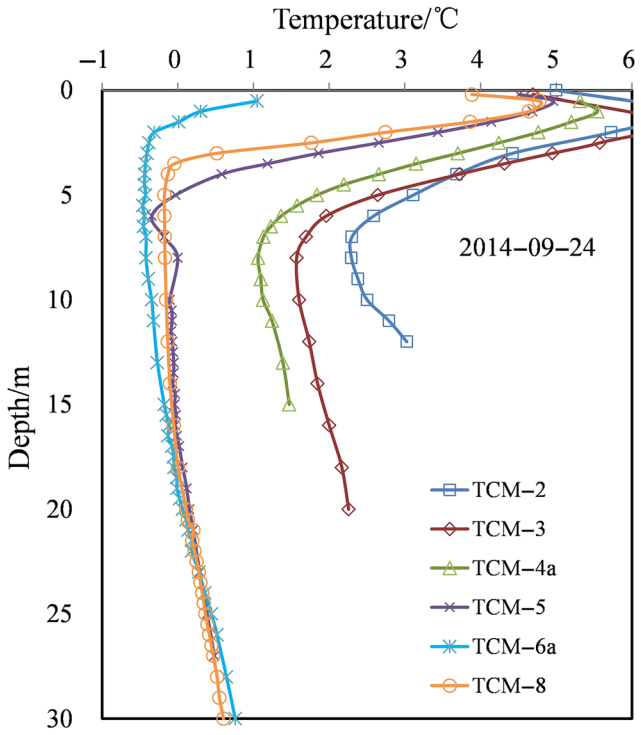

FIGURE 12 Ground temperature curve of permafrost borehole in Tangchama [Colour figure can be viewed at wileyonlinelibrary.com]

degradation in the HAYR is 7.5–8.6% by 2050 and 32.9–62.2% by 2100. Although the predictions of permafrost are highly uncertain, due to different climate models, the trend of permafrost degradation is the same. This study derives the permafrost changes under different climate scenarios. Although temperature increase in the new generation scenarios RCP2.6, RCP6.0, and RCP8.5 in IPCC, AR5 is the mean of the multimode simulation results; the simulation results under different scenarios can provide a deeper understanding of the future changes of permafrost. This study provides different approaches to predicting permafrost change.

Many studies mainly focus on the distribution and evolution of permafrost in the Qinghai-Tibet Plateau (Guo et al., 2012; Wang, Yang, Yang, Qin, & Wang, 2018). Influenced by the spatial scale effect, the permafrost distribution of the HAYR is simplified in these studies. Moreover, previous studies have not systematically accounted for the distribution and evolution of permafrost in the HAYR. Air temperature is not the only influencing factor of permafrost. Landforms, lithology, and geology, among many others, could significantly affect the hydrothermal state of permafrost. This study further considers the influence of topographic factors and lithology factors on the change of permafrost in the HAYR. In this study, the permafrost classification is firstly refined at large scale. According to geomorphic units and stratum features in the HAYR, permafrost was categorized into four types, LICHPP, HICHPP, LICAP, and HICAP. Therefore, this study better reflects the differences and diversity of the spatial distribution of permafrost. In addition, this study was validated via comparison to a large number of field borehole monitoring data of permafrost in the HAYR. Therefore, compared with previous studies, this work more accurately predicts the permafrost distribution in the HAYR. The permafrost change derived from this study is similar to the estimates from the many previous studies.

5.3 | Feasibility and deficiency of the method

The time series of the ground temperature measurements are much shorter than the timescale of permafrost degradation. Thus, the permafrost degradation process, under complex situations, can only be effectively studied by numerical model simulations. The temperature conditions of the upper and lower boundaries, as well as heat transfer in the strata, were simplified by using a model based on thermal conduction theory. The model can be used to describe the transfer of heat in the permafrost strata to describe the delayed permafrost response to climate changes. It also has advantages in simulating permafrost changes at different depths. The simulated depth reached 100 m, which effectively reveals the impact of centennial climate change on permafrost at various depths. The model provides an in-depth understanding of the temperature change process of deep permafrost layers, greater than 50–100 m. Soil temperature dynamics were simulated with the upper boundary condition determined by the surface energy balance and the lower boundary condition (at a depth of 120 m) determined by the geothermal heat flux (Zhang & Chen, 2003). This method is well used in the field of permafrost engineering. Compared with numerical modeling, the land-surface process model is useful for describing surface processes that include numerous physical mechanisms. However, it does not account for deep permafrost responses, at more than 10 m (Lawrence & Slater, 2005; Guo, Wang, & Li, 2012). Thus, it cannot be used to investigate the entire permafrost degradation process. Therefore, coupling the improved land-surface process model with global or regional climate models, for predicting the permafrost change processes and response mechanisms under a warming climate is a more effective and accurate tool.

6 | CONCLUSIONS

A numerical model simulation was performed for four typical permafrost types in the HAYR region on northeastern Qinghai-Tibet Plateau, Southwest China. Changes in the distribution of permafrost in the past and future were mapped by using GIS platform-aided numerical models. The conclusions can be drawn as follows:

1. During permafrost degradation, the same type permafrost at different degradation stages experiences different modes and rates of increasing temperature. The responses of permafrost to climate change would differ in stages of thermal regimes. For different permafrost types with similar MAGTs, the rate of permafrost degradation depends on sensitivity to lithology, ice content, and some other influencing factors. The greater the ground ice content, the lower the rate of permafrost degradation.
2. From 1972 to 2012, the area of permafrost degradation was 1,056 km^2, resulting from a sharp temperature increase after the 1980s.

By 2050, the areas of permafrost thaw would be similar under the three scenarios of RCP2.6, RCP6.0, and RCP8.5. The areas of permafrost degradation would be 2,224, 2,347, and 2,559 km^2, which accounts for 7.5%, 7.9%, and 8.6% of the total area in the HAYR, under the three scenarios, respectively. In RCP2.6, the areal extent of permafrost degradation into seasonal frost by 2100 would be approximately 3,500 km^2. Under the scenario RCP6.0, the area of permafrost thaw by 2100 would be 10,000 km^2, 32.9% of the total area in the HAYR. Under the scenario RCP8.5, the area of permafrost degradation by 2100 would be 18,492 km^2, 62.2% of the total area in the HAYR. Moreover, the average ALT was 1.51 m in 1972 and 2.01 m in 2012. Under the RCP2.6, RCP6.0, and RCP8.5 scenarios, the basin-wide average of ALT would be 2.21, 2.40, and 3.08 m by 2050 and 2.78, 4.07, and 4.39 m by 2100, respectively.

3. In the spatial expansion of permafrost distribution, this study simply used 0°C as the basis for boundary division between seasonal frozen soil and permafrost. This assumption may result in the misclassification of shallow thin permafrost or buried permafrost as seasonally frozen soil. This is because the ground temperature of shallow thin and buried permafrost is positive above 15 m in depth and negative above or below 15 m in depth. Therefore, these soils are not classified as permafrost in the statistical process. This requires more field data to verify the calculation results in the future. In addition, the model simply considers the temperature rise at the upper boundary in the calculation of the ALT. However, the ALT is related to many other factors such as surface vegetation, soil texture, atmospheric temperature, and permafrost table. In the future, the model should include a series of meteorological elements, surface soil, and vegetation parameters to study the ALT based on the land surface process model.

ACKNOWLEDGMENTS

This research was supported by the National Natural Science Foundation of China (Grants 91647103 and 41971093), the subproject of the Strategic Priority Research Program of Chinese Academy of Sciences (CAS) (Grant XDA20100103), and the self-determined Project Funded by State Key Laboratory of Frozen Soil Engineering (SKLFSE-ZQ-43). The authors thank the editors and anonymous reviewers for their insightful comments and suggestions that helped improve this paper.

ORCID

Wei Cao https://orcid.org/0000-0003-2963-267X

REFERENCES

Azócar, G. F., Brenning, A., & Bodin, X. (2017). Permafrost distribution modelling in the semi-arid chilean andes. *The Cryosphere*, *11*(2), 877–890. https://doi.org/10.5194/tc-11-877-2017

Cao, Y. B., Sheng, Y., Wu, J. C., Li, J., Ning, Z. J., & Hu, X. Y. (2014). Influence of upper boundary conditions on simulated ground temperature field in permafrost regions. *Journal of Glaciology and Geocryology*, *36*(4), 802–810. https://doi.org/10.7522/j.issn.1000-0240.2014.0096

Catherine, S. M., Hoelzle, M., & Haeberli, W. (2002). Modelling alpine permafrost distribution based on energy-balance data: A first step. *Permafrost and Periglacial Processes*, *13*(4), 271–282. https://doi.org/10.1002/ppp.426

Fang, H. B., Zhao, F. Y., & Sun, Y. G. (2009). *Crustal movement and sedimentary response in quaternary period on the Qinghai-Tibet Plateau* (pp. 3–30). Beijing, China: Geological Publishing House.

Frey, K. E., & Mcclelland, J. W. (2010). Impacts of permafrost degradation on arctic river biogeochemistry. *Hydrological Processes*, *23*(1), 169–182. https://doi.org/10.1002/hyp.7196

GB50324-2001. (2014). Code for engineering geological investigation of frozen ground. Beijing: China Planning Press.

Guo, D. L., Wang, H. J., & Li, D. (2012). A projection of permafrost degradation on the Tibetan plateau during the 21st century. *Journal of Geophysical Research-Atmospheres*, *117*(D5), 214–221. https://doi.org/10.1029/2011JD016545

Jin, H. J., He, R. X., Cheng, G. D., Wu, Q. B., Wang, S. L., Liu, L. Z., & Chang, X. L. (2009). Changes in frozen ground in the Source Area of the Yellow River on the Qinghai-Tibet Plateau, China, and their eco-environmental impacts. *Environmental Research Letters*, *4*(4), 1–11. https://doi.org/10.1088/1748-9326/4/4/045206

Jin, H. J., Zhao, L., Wang, S. L., & Jin, R. (2006). Thermal regimes and degradation modes of permafrost along the Qinghai-Tibet Highway. *Science in China Series D-Earth Sciences*, *49*(11), 1170–1183. https://doi.org/10.1007/s11430-006-2003-z

Jorgenson, M. T., Racine, C. H., Walters, J. C., & Osterkamp, T. E. (2001). Permafrost degradation and ecological changes associated with a warming climate in Central Alaska. *Climatic Change*, *48*(4), 551–579. https://doi.org/10.1023/A:1005667424292

Jorgenson, M. T., Shur, Y. L., & Pullman, E. R. (2006). Abrupt increase in permafrost degradation in Arctic Alaska. *Geophysical Research Letters*, *33*(2), 356–360. https://doi.org/10.1029/2005GL024960

Koven, C. D., Ringeval, B., Friedlingstein, P., Ciais, P., Cadule, P., & Khvorostyanov, D. (2011). Permafrost carbon-climate feedbacks accelerate global warming. *Proceedings of the National Academy of Sciences of the United States of America*, *108*(36), 14769–14774. https://doi.org/10.1073/pnas.1103910108

Lawrence, D. M., & Slater, A. G. (2005). A projection of severe near-surface permafrost degradation during the 21st century. *Geophpysical Research Letters*, *32*(24), 230–250. https://doi.org/10.1029/2005GL025080

Li, J., Sheng, Y., Wu, J. C., Feng, Z. L., Ning, Z. J., & Hu, X. Y. (2016). Mapping frozen soil distribution and modeling permafrost stability in the source area of the Yellow River. *Scientia Geographica Sinica*, *36*(4), 588–596. https://doi.org/10.13249/j.cnki.sgs.2016.04.013

Li, S. X., Cheng, G. D., & Guo, D. X. (1996). The future thermal regime of numerical simulating permafrost on Qinghai-Xizang (Tibet) Plateau, China, under climate warming. *Science China: Earth Sciences*, *26*(4), 342–347. https://doi.org/10.1016/0268-0033(95)00021-6

Li, X., & Cheng, G. D. (1999). A GIS-aided response model of high altitude permafrost to global change. *Science China: Earth Sciences*, *42*(1), 72–79. https://doi.org/10.1007%2FBF02878500

Li, X., Cheng, G. D., Jin, H. J., Kang, E., Che, T., & Jin, R. (2008). Cryospheric change in China. *Global and Planetary Change*, *62*(3-4), 210–218. https://doi.org/10.1016/j.gloplacha.2008.02.001

Lu, Q., Zhao, D. S., & Wu, S. H. (2017). Simulated responses of permafrost distribution to climate change on the Qinghai-Tibet Plateau. *Scientific Reports*, *7*(1), 3845. https://doi.org/10.1038/s41598-017-04140-7

Nan, Z. T., Li, S. X., & Cheng, G. D. (2005). Prediction of permafrost distribution on the Qinghai-Tibet Plateau in the next 50 and 100 years. *Science China: Earth Sciences*, *48*(6), 797–804. https://doi.org/10.1360/03yd0258

Nelson, F. E. (1986). Permafrost distribution in central Canada: Applications of a climate-based predictive model. *Annals of the Association of American Geographers*, *76*, 550–569. https://doi.org/10.1111/j.1467-8306.1986.tb00136.x

Nelson, F. E. (1987). A computational method for prediction and regionalization of permafrost. *Arctic and Alpine Research*, *19*(3), 279–288. https://doi.org/10.2307/1551363

Nguyen, T. N., Burn, C. R., King, D. J., & Smith, S. L. (2009). Estimating the extent of near-surface permafrost using remote sensing, Mackenzie Delta, Northwest Territories. *Permafrost and Periglacial Processes*, *20*(2), 141–153. https://doi.org/10.1002/ppp.637

Niu, F. J., Yin, G. A., Luo, J., Lin, Z. J., & Lin, M. H. (2018). Permafrost distribution along the Qinghai-Tibet engineering corridor, China using high-resolution statistical mapping and modeling integrated with remote sensing and GIS. *Remote Sensing*, *10*(2), 215. https://doi.org/10.3390/rs10020215

Osterkamp, T. E., & Romanovsky, V. E. (2015). Evidence for warming and thawing of discontinuous permafrost in Alaska. *Permafrost and Periglacial Processes*, *10*(1), 17–37. https://doi.org/10.1002/(SICI)1099-1530(199901/03)10:1<17::AID-PPP303>3.0.CO;2-4

Ran, Y. H., Li, X., & Cheng, G. D. (2018). Climate warming over the past half century has led to thermal degradation of permafrost on the Qinghai–Tibet Plateau. *The Cryosphere*, *12*(2), 595–608. https://doi.org/10.5194/tc-12-595-2018

Ran, Y. H., Li, X., Cheng, G. D., Zhang, T. J., Wu, Q. B., & Jin, H. J. (2012). Distribution of permafrost in China: An overview of existing permafrost maps. *Permafrost and Periglacial Processes*, *23*(4), 322–333. https://doi.org/10.1002/ppp.1756

Riseborough, D., Shiklomanov, N., EtzelmÜLler, B., Gruber, S., & Marchenko, S. (2010). Recent advances in permafrost modelling. *Permafrost and Periglacial Processes*, *19*(2), 137–156. https://doi.org/10.1002/ppp.615

Schuur, E. A., McGuire, A. D., Schädel, C., Grosse, G., Harden, J. W., Hayes, D. J., … Natali, S. M. (2015). Climate change and the permafrost carbon feedback. *Nature*, *520*(7546), 171–179. https://doi.org/10.1038/nature14338

Shur, Y. L., & Jorgenson, M. T. (2010). Patterns of permafrost formation and degradation in relation to climate and ecosystems. *Permafrost and Periglacial Processes*, *18*(1), 7–19. https://doi.org/10.1002/ppp.582

Stocker, T. F., Qin, D.H., Plattner, G. K., Tignor, M., Allen, S. K., Boschung, J., … Midgley, P. M. (2013). IPCC, 2013: Climate change 2013: The physical science basis. *Contribution of working Group I to the Fifth Assessment Report of the Intergovernmental Panel on Climate Change*, 710-719. https://doi.org/10.1017/CBO9781107415324

Su, F., Duan, X. L., Chen, D. L., Hao, Z. C., & Cuo, L. (2013). Evaluation of the global climate models in the CMIP5 over the Tibetan Plateau. *Journal of Climate*, *26*(10), 3187–3208. https://doi.org/10.1175/JCLI-D-12-00321.1

Tanarro, L. M., Hoelzle, M., García, A., Ramos, M., Gruber, S., Gómez, A., … Palacios, D. (2001). Permafrost distribution modeling in the mountains of the Mediterranean: Corral del Veleta, Sierra Nevada, Spain. *Norwegian Journal of Geography*, *55*(4), 253–260. https://doi.org/10.1080/00291950152746612

Wang, J. C., & Li, S. D. (1983). *Analysis of thermal regime near the permafrost floor surface along Qinghai-Tibet Highway. Professional Papers on Permafrost Studies of Qinghai-Xizang Plateau* (pp. 38–43). Beijing: Science Press.

Wang, S. L., Jin, H. J., Li, S. X., & Zhao, L. (2000). Permafrost degradation on the Qinghai–Tibet Plateau and its environmental impacts. *Permafrost and Periglacial Processes*, *11*(1), 43–53. https://doi.org/10.1002/(SICI)1099-1530(200001/03)11:13.0.CO;2-H

Wang, S. T., Sheng, Y., Li, J., Wu, J. C., Cao, W., & Ma, S. (2018). An estimation of ground ice volumes in permafrost layers in northeastern Qinghai-Tibet Plateau, China. *Chinese Geographical Science*, *28*(1), 61–73. https://doi.org/10.1007/s11769-018-0932-z

Wang, T. H., Yang, D. W., Fang, B. J., Yang, W. C., Qin, Y., & Wang, Y. H. (2019). Data-driven mapping of the spatial distribution and potential changes of frozen ground over the Tibetan Plateau. *Science of the Total Environment*, *649*, 515–525. https://doi.org/10.1016/j.scitotenv.2018.08.369

Wang, T. H., Yang, H. B., Yang, D. W., Qin, Y., & Wang, Y. H. (2018). Quantifying the streamflow response to frozen ground degradation in the source region of the Yellow River within the Budyko framework. *Journal of Hydrology*, *558*, 301–313. https://doi.org/10.1016/j.jhydrol.2018.01.050

Wang, W., Rinke, A., Moore, J. C., Cui, X., Ji, D., Li, Q., … Decharme, B. (2016). Diagnostic and model dependent uncertainty of simulated Tibetan permafrost area. *The Cryosphere*, *10*, 287–306. https://doi.org/10.5194/tc-10-287-2016

Wu, J. C., Sheng, Y., Wu, Q. B., & Wen, Z. (2010). Processes and modes of permafrost degradation on the Qinghai-Tibet Plateau. *Science China: Earth Sciences*, *53*(1), 150–158. https://doi.org/10.1007/s11430-009-0198-5

Wu, Q. B., Zhang, T. J., & Liu, Y. Z. (2010). Permafrost temperatures and thickness on the Qinghai-Tibet Plateau. *Global and Planetary Change*, *72*(1-2), 32–38. https://doi.org/10.1016/j.gloplacha.2010.03.001

Wu, X. B., Nan, Z. T., Zhao, S. P., & Cheng, G. D. (2018). Spatial modeling of permafrost distribution and properties on the Qinghai-Tibet Plateau. *Permafrost and Periglacial Processes*, *29*(2), 86–99. https://doi.org/10.1002/ppp.1971

Xu, X. Z., Wang, J. C., & Zhang, L. X. (2001). *Permafrost physics* (pp. 43–62). Beijing: Science Press.

Yang, M. X., Nelson, F. E., Shiklomanov, N. I., Guo, D. L., & Wan, G. N. (2010). Permafrost degradation and its environmental effects on the Tibetan Plateau: A review of recent research. *Earth Science Reviews*, *103*(1), 31–44. https://doi.org/10.1016/j.earscirev.2010.07.002

Zhang, L., Ding, Y. H., Wu, T. W., Xin, X. G., Zhang, Y. W., & Xu, Y. (2013). The 21st century annual mean surface air temperature change and the 2°C warming threshold over the globe and China as projected by the CMIP5 models. *Acta Meteorologica Sinica*, *71*(6), 1047–1060. https://doi.org/10.11676/qxxb2013.087

Zhang, Y., & Chen, W. J. (2003). A process-based model for quantifying the impact of climate change on permafrost thermal regimes. *Journal of Geophysical Research*, *108*(D22), 4695. https://doi.org/10.1029/2002jd003354

Zhao, S. P., Nan, Z. T., Huang, Y. B., & Zhao, L. (2017). The application and evaluation of simple permafrost distribution models on the Qinghai–Tibet Plateau. *Permafrost and Periglacial Processes*, *28*(2), 391–404. https://doi.org/10.1002/ppp.1939

Zhou, C. H., Cheng, W. M., Zhao, S. M., Gao, X. Y., & Nan, W. (2007). *Geomorphological map of Western China (1:1000000)*. Beijing: Institute of Geographic Sciences and Natural Resources Research, Chinese Academy of Sciences.

Zimov, S. A., Schuur, E. A., & Chapin, F. S. (2006). Permafrost and the global carbon budget. *Science*, *312*(5780), 1612–1613. https://doi.org/10.1126/science.1128908

Zou, D., Zhao, L., Yu, S., Chen, J., Hu, G., Wu, T., … Wang, W. (2017). A new map of permafrost distribution on the Tibetan Plateau. *The Cryosphere*, *11*(6), 2527–2542. https://doi.org/10.5194/tc-11-2527-2017

How to cite this article: Sheng Y, Ma S, Cao W, Wu J. Spatio-temporal changes of permafrost in the Headwater Area of the Yellow River under a changing climate. *Land Degrad Dev*. 2020;31:133–152. https://doi.org/10.1002/ldr.3434